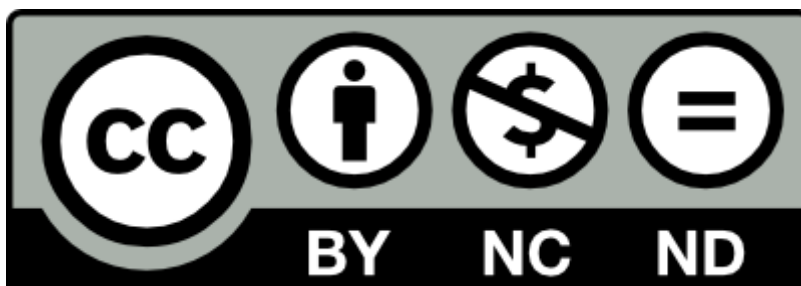


Amaia Morales, Jalel Labidi, Patricia Gullón, Assessment of green approaches for the synthesis of physically crosslinked lignin hydrogels, *Journal of Industrial and Engineering Chemistry* 81, 2020, Pages 475-487, Online ISSN: 1876-794X, <https://doi.org/10.1016/j.jiec.2019.09.037>.

(<https://www.sciencedirect.com/science/article/pii/S1226086X19305155?pes=vor>)

Abstract: Lignin is an excellent candidate to be used as a start material for hydrogel synthesis due to its highly functional character. The exhaustible character of the fossil resources linked to the increase of plastic residues on the environment encourage an intensive research on biorenewable and biodegradable polymers to synthesize new materials. Taking into account this current scenario, this work searches new green routes to elaborate physical hydrogels with excellent capacity of swelling and suitable consistency. To this end, lignin and poly (vinyl alcohol) were blended in different proportions following a three-level-two-factorial design and using six different routes of crosslinking and drying for each set of experiments. The hydrogels formed under the optimal conditions were characterized by FTIR, SEM, XRD, DSC and TGA and their mechanical properties were also evaluated by compression tests. The selected optimum synthesis routes enabled the obtaining of physically crosslinked hydrogels with up to 800 % water retention ability. FTIR spectra confirmed the interactions between lignin and PVA showing shifts and modifications on the characteristics bands of the raw polymers. Compression tests showed that all the hydrogels kept complete integrity even compressing them up to an 80 % of their initial thickness.

Keywords: lignin, poly (vinyl alcohol), physical crosslinking, hydrogels, swelling, mechanical properties



**Assessment of green approaches for the synthesis of physically crosslinked lignin
hydrogels**

Amaia Morales, Jalel Labidi*, Patricia Gullón

Chemical and Environmental Engineering Department, University of the Basque Country
UPV/EHU, Plaza Europa 1, 20018, San Sebastián, Spain

*Corresponding author: jalel.labidi@ehu.es

Abstract

Lignin is an excellent candidate to be used as a start material for hydrogel synthesis due to its highly functional character. The exhaustible character of the fossil resources linked to the increase of plastic residues on the environment encourage an intensive research on biorenewable and biodegradable polymers to synthesize new materials. Taking into account this current scenario, this work searches new green routes to elaborate physical hydrogels with excellent capacity of swelling and suitable consistency. To this end, lignin and poly (vinyl alcohol) were blended in different proportions following a three-level-two-factorial design and using six different routes of crosslinking and drying for each set of experiments. The hydrogels formed under the optimal conditions were characterized by FTIR, SEM, XRD, DSC and TGA and their mechanical properties were also evaluated by compression tests. The selected optimum synthesis routes enabled the obtaining of physically crosslinked hydrogels with up to 800 % water retention ability. FTIR spectra confirmed the interactions between lignin and PVA showing shifts and modifications on the characteristics bands of the raw polymers. Compression tests showed that all the hydrogels kept complete integrity even compressing them up to an 80 % of their initial thickness.

Keywords: lignin, poly (vinyl alcohol), physical crosslinking, hydrogels, swelling, mechanical properties

1. Introduction

Lignocellulosic biomass is mainly composed of carbohydrate polymers (cellulose and hemicellulose), and aromatic polymers (lignin and tannin) [1]. In recent years, these biorenewable polymers have attracted a greater attention of the research community due to the advantages such as eco-friendliness, low cost, biodegradability, etc.

Among these biorenewable polymers, lignin is the second most abundant and fascinating natural polymer next to cellulose. Lignin is primarily composed of three different phenylpropane units, namely, p-coumaryl, coniferyl and sinapyl alcohols. Different types of carbon–carbon/and carbon–oxygen bonds are formed between different monomer units in lignin [2]. Lignin can be obtained as a byproduct of the pulp and paper industry, bio-ethanol production and can be specifically generated in new biorefinery schemes [3], however, it is often burnt to generate energy for the process. Nevertheless, if added-value applications were searched for lignin, an integral valorisation of the lignocellulosic feedstock would be enabled and, hence, biorefineries would contribute to a circular economy.

The impressive properties of lignin, such as its high abundance, antioxidant, antimicrobial, and biodegradable nature, along with its CO₂ neutrality and reinforcing capability, make it an excellent candidate for chemical modifications and reactions as well as for the development of new biobased materials [4]. Lignin is, therefore, a cost environmental friendly feedstock with a great potential to be used as a start material for hydrogel synthesis due to its highly functional character (i.e., rich in phenolic and aliphatic hydroxyl groups).

Hydrogels are three-dimensionally crosslinked polymeric networks with high water retention capacity which have significantly gained attention over the last 20 years [5]. They have been employed in many fields such as biomedicine or agriculture and they have become very interesting materials due to their adequate physic-chemical characteristics for many applications [6]. According to the type of crosslinking, they can be classified as physical (with physical entanglements or secondary forces) or chemical (with covalent bondages) hydrogels [5]. Chemical crosslinking is the highly resourceful method for the formation of hydrogels having an excellent mechanical strength but the crosslinkers used in hydrogel preparation should be

extracted from the hydrogels before use due to their reported toxicity, which is a considerable inconvenience. Physical crosslinking methods for the preparation of hydrogels are the alternative solution to crosslinkers' toxicity and cost. They are usually formed by hydrogen bondages and electrostatic, hydrophobic and host-guest interactions [7]. However, due to the weak nature of these forces, these hydrogels are also known as reversible hydrogels and sometimes disintegrate and dissolve in water [8] and they can also be thermally reversible [9]. Nevertheless, the weakness problem can be solved by supramolecular chemistry [7,10] and the reversibility can be an advantage when talking about self-healable hydrogels, which have gained great interest in the last years [11,12]. Therefore, it is clear that physically crosslinked hydrogels present several benefits that chemically crosslinked ones do not, enabling at the same time a greener and a more economical synthesis process [13].

The increase of concern about the environmental and health impacts caused by the use of non-biodegradable polymers produced from fossil resources requires an urgent shift to renewable carbon-resource. This is why the possibility of synthesizing bio-based hydrogels has been investigated recently. The abundance and the cheapness of lignin, as well as the need to revalorize it, have made lignin attractive to employ as a backbone polymer for hydrogel synthesis. Some authors have already incorporated lignin into hydrogels [14,15], but as it has a complex structure, it is difficult to design precise synthesis and obtain materials with the desired properties. Nevertheless, in spite of their brownish colour, the applicability of the lignin-based hydrogels is considerably wide (see Table 1). However, in most of the cases, chemical crosslinking has been performed and, hence, toxic reagents have been employed [2].

According to the aforementioned, the aim of this work was to find the optimum synthesis route to produce physical hybrid hydrogels based on biodegradable polymers via a greener synthesis route, avoiding the use of toxic chemical reagents. To this end, lignin was blended with poly(vinyl alcohol) (PVA), which is a biodegradable and non-toxic synthetic polymer [16]. In this way, the interactions between both components in the blend would enable the generation of highly hydrophilic three-dimensional networks. An experimental design was employed as the basis of

the hydrogel synthesis, with lignin and PVA concentrations as input variables and lignin waste and swelling rate as output dependent variables. Three levels of the input variables were studied, which led to a factorial design of 3 levels, 3^2 , with a triplicate central point. Eleven experiments were designed and they were subjected to six different synthesis pathways, varying the crosslinking method and curing method, in order to obtain the optimal lignin and PVA concentrations as well as the better synthesis routes to minimize the lignin waste and maximize the swelling rate. The accuracy of the six models was then evaluated by statistical analysis and, after selecting the best models, the hydrogels formed under the optimal conditions were characterized by Attenuated Total Reflection-Fourier Transformed Infrared Radiation (FTIR), Scanning Electron Microscopy (SEM), X-Ray Diffraction (XRD), Differential Scanning Calorimetry (DSC) and Thermogravimetric Analysis (TGA). Their mechanical properties were also evaluated by compression tests.

2. Materials and Methods

2.1. Materials

Alkaline lignin and poly (vinyl alcohol) (PVA, $M_w=83,000-124,000$ g/mol, 99+ % hydrolyzed) were supplied by Sigma Aldrich. Sodium hydroxide (NaOH, analysis grade, $\geq 98\%$, pellets) was purchased from PanReac Química SLU. All reagents were employed as supplied.

2.2. Hydrogel Synthesis

Different hydrogels were synthesized according to the combinations designed by an experimental model (see section 2.3.), in which the input variables were both the lignin and the PVA concentrations. All the hydrogels were prepared by adding the corresponding PVA amount (5, 8 or 11 % (w/w)), i.e. 0.5, 0.8 or 1.1 g of PVA to 10 mL of a 2 % NaOH aqueous solution, which was magnetically stirred and heated to 80-90°C simultaneously. When the PVA pellets were dissolved, the corresponding amount of lignin (5, 15 or 25% (w/w), i.e. 0.5, 1.5 or 2.5 g) was incorporated under agitation until it was completely dissolved. Defined amounts of the blends were poured into silicon moulds and the bubbles on the surface were poked manually with a

needle, while the ones trapped into the solution were eliminated by introducing the moulds into an ultrasound bath.

In order to study the influence of the synthesis paths, the blends were subjected to three different crosslinking (XL) methods: 3 and 5 cycles of freeze-thawing (16 h at -20 °C and 8 h at 28 °C) and inside a vacuum hood at 37 °C (-60 cm Hg) for a week. After the crosslinking stage, the hydrogels were separately washed into 50 mL of distilled water with orbital shaking several times. The washing was performed so as to eliminate the non-reacted lignin and the residual NaOH. Afterwards, the hydrogels were dried in two different ways: half of them were left to dry at room temperature while the other half dried under vacuum (-60 cm Hg) at 27 °C. These two drying or curing methods were employed in order to observe the influence of this stage (Figure 1).

The hydrogels with the optimal compositions were prepared similarly employing the corresponding amounts of lignin and PVA into 15 mL of a 2 % NaOH solution.

(Figure 1)

The six synthesis routes depicted in Figure 2 represent the following used paths:

- (1) Vacuum XL + Air Drying (Vac-Air)
- (2) Vacuum XL + Vacuum Drying (Vac-Vac)
- (3) 5 cycles of Freeze-Thawing XL + Air Drying (F-T x5-Air)
- (4) 5 cycles of Freeze-Thawing XL + Vacuum Drying (F-T x5-Vac)
- (5) 3 cycles of Freeze-Thawing XL + Air Drying (F-T x3-Air)
- (6) 3 cycles of Freeze-Thawing XL + Vacuum Drying (F-T x3-Vac)

(Figure 2)

2.3. Model Description

Three-level-two-factorial design with three replicates in the central point and a Response Surface Methodology (RSM) were employed to perform the optimization of the conditions of the lignin-hydrogel synthesis. The selected independent variables were both the alkaline lignin (x_1) and the

PVA concentrations (x_2), which ranged from 5 to 25% (w/w) and from 5 to 11% (w/w), respectively. These ranges were chosen in the basis of previous experiments (data not shown). The response variables were the swelling capacity of the hydrogels (% , y_1) and the lignin waste during the washing stage (% , y_2). Moreover, the accuracy of each of the models would also help to select the best synthesis route. Eleven experiments were designed for each pathway considering the selected parameter values and the triplicate central point (see Table 2), so sixty six experiments were carried out in total. Experimental data were fitted using a second-order polynomial described by the Equation (1):

$$y_j = \beta_0 + \beta_1 x_1 + \beta_2 x_2 + \beta_{11} x_1^2 + \beta_{22} x_2^2 + \beta_{12} x_1 x_2 \quad (1)$$

where y_j are the dependent variables ($j = 1-2$), β_0 , β_1 , β_2 , β_{11} , β_{22} and β_{12} are the regression coefficients calculated from the experimental results by the least-squares method, and x_1 and x_2 are the dimensionless, normalized independent variables, with variation ranges from -1 to 1 . Experimental data were fitted using the regression analysis function of Microsoft Excel's Data Analysis Add-In, USA. The adequacy of the model was determined by evaluating the lack of fit, the coefficient of determination (R^2) and the F-test value obtained from the analysis of variance.

To generate the experimental design, the statistical analysis and the regression model, Statgraphics Centurion version XVI (Statpoint Technologies Inc., Warrenton, VA, USA) software was employed. The figures were reproduced using OriginPro®9 (OriginLab Corp., Northampton, MA, USA). The models were validated by carrying out the experiments at the optimal points and comparing the results obtained experimentally with the predicted data.

2.4. Hydrogel Characterization

2.4.1. Lignin Waste

First, a calibration curve was performed by employing five lignin solutions (10 mL) prepared in 2 % (w/w) NaOH with known concentrations (0.25, 0.5, 1.5, 2.5 and 5.0 mg lignin/mL solution) and a V-630 UV-Jasco spectrophotometer. In order to fix the correct wavelength to measure the absorbance of the samples, a preliminary scan was performed from 760 to 250 nm. Thus, the

measurements were done at 515 nm and each absorbance was related to the concentration of the prepared dissolutions. In this way, a calibration curve was obtained, which corresponded to Equation (2):

$$A_{515nm} = 0.7643 \cdot [Lignin] \quad (2)$$

The hydrogels were washed in 50 mL of distilled water until the water was clear, for 24-30 hours approximately. During the washing stage, aliquots were taken each time and the washing water was changed every 2-3 h. The concentrations of the aliquots were calculated from the measured absorbance at 515 nm. Finally, taking the volume of each rinse into account, the total lignin loss was calculated.

2.4.2. Swelling

The hydrogels were weighted in dry state and immersed in 40 mL of distilled water for 48 hours. For the swelling kinetics, the hydrogels were weighted at certain times, removing the water remaining on the surface with filter paper. The swelling degree was calculated from the following Equation (3) [6]:

$$Swelling (\%) = \frac{m_{swollen} - m_{dry}}{m_{dry}} \cdot 100 \quad (3)$$

in which $m_{swollen}$ and m_{dry} are the masses of swollen and dried hydrogels, respectively.

2.4.3. Attenuated Total Reflection - Fourier Transformed Infrared Radiation (ATR-FTIR):

In order to study and verify the interactions between the polymers, a PerkinElmer Spectrum Two FT-IR Spectrometer equipped with a Universal Attenuated Total Reflectance accessory with internal reflection diamond crystal lens was used to collect Infrared spectra of the hydrogels. The studied range was from 600 to 4000 cm^{-1} and the resolution was 8 cm^{-1} . 20 scans were recorded for each grated dry sample.

2.4.4. Scanning Electron Microscopy (SEM)

SEM analyses were carried out in order to study the morphology of the hydrogels. The samples were swollen in water for 48 hours at room temperature and then frozen at -20°C. Afterwards, they were freeze-dried in an Alpha 1-4 LD freeze drier. The images of secondary electrons were taken with a MEB JEOL 7000-F. The working conditions were 5 kV and an intensity of 0.1 nA. The samples were covered with 20 nm of Cr by sputtering technique.

2.4.5. X-Ray Diffraction (XRD)

X-Ray Powder diffraction tests were carried out using a Phillips X'Pert PRO automatic diffractometer operating at 40 kV and 40 mA, in theta-theta configuration. Monochromatic Cu-K α ($\lambda=1.5418$ Å) radiation and a PIXcel solid-state detector (active length in 2θ 3.347°) were employed. The collected data ranged from 5 to 80° 2θ at room temperature. The step size was 0.026 and the time per step was 80 s. 0.04 rad soller slit and fixed 1° divergence slit giving a constant volume of sample illumination were employed. The samples were subjected to XRD analysis grated and in dry state.

The approximate size (D) of crystallites was calculated using the Scherrer equation (Eq. 4):

$$D = \frac{k \cdot \lambda}{\beta \cdot \cos \theta} \quad (4)$$

Where D is the mean size of ordered domains (nm), k is the Scherrer constant (0.9), λ is the X-ray wavelength (0.154 nm) and β is the full-width at half-maximum of the reflection (FWHM) measured in 2θ of the corresponding Bragg angle [17,18].

2.4.6. Differential Scanning Calorimetry (DSC)

DSC analyses were done on a Mettler Toledo DSC 822 (Mettler Toledo, Spain). Between 3-5 mg of dry grated samples were subjected to a heating ramp from -25 °C to 225 °C at a rate of 10 °C/min under nitrogen atmosphere to avoid oxidative reactions inside aluminium pans. After the first heating step, cooling and second heating stages were also performed. The glass transition temperature (T_g), was considered as the inflection point of the specific heat increment during the second heating scan. The calibration was performed with indium standard. The degree of

crystallinity (χ_c) was obtained from the enthalpy evolved during crystallization using Equation (5)[19] :

$$\chi_c = \frac{\Delta H}{\Delta H_0 \cdot (1 - m_{\text{filler}})} \cdot 100 \quad (5)$$

where ΔH , is the apparent enthalpy for melting or crystallization, ΔH_0 is the melting enthalpy of 100% crystalline PVA (average value: 161.6 J/g) and $(1 - m_{\text{filler}})$ is the weight percent of PVA in the hydrogels [19].

2.4.7. Thermogravimetric Analysis (TGA)

TGA analyses were done on a TGA/SDTA 851 Mettler Toledo (Mettler Toledo, Spain) instrument. Around 7 mg of dry grated sample were subjected to a heating ramp of 25 °C/min from room temperature up to 800 °C under a nitrogen atmosphere inside platinum pans.

2.4.8. Compression studies

Uniaxial compression tests were performed on the hydrogels in order to assess their mechanical strength. A compression gear was set up on an Instron 5967 machine using a 500 N load cell with a crosshead speed of 2 mm/min. Square samples of around 5 x 5 mm were cut from the initial hydrogels, which were left to swell during 48 h at room temperature. Then, the samples were compressed up to the 80% of their initial thickness. This strain was selected according to other works and the limitations of the compression test equipment caused by the thicknesses of the samples [Kalinowski_2019]. The swollen modulus, G_e , of each sample was calculated automatically by employing Eq. 6. [20,21]

$$\sigma = \frac{F}{A} = G_e \cdot \left(\lambda - \frac{1}{\lambda^2} \right) \quad (6)$$

Where F is the force, A is the original cross sectional area of the swollen hydrogel, and $\lambda = L/L_0$ where L_0 and L are the thicknesses of the samples before and after compression, respectively.

3. Results and Discussion

3.1. Modelling and Optimization of Hydrogel Composition

In order to obtain the best hydrogel formulations and the best synthesis route, the optimization of the input variables was addressed using the three-level-two-factorial design combined with Response Surface Methodology for the six synthesis pathways. The results for the all the measured swelling capacities and lignin wastes are shown in Table 3. The six optimal concentrations for the maximum swelling and the minimum lignin waste calculated by the software, as well as the predicted values for the response variables, are shown in Table 4. The optimal conditions of the six paths were verified by the triplicate synthesis of the hydrogels.

Table 5 shows the regression coefficients obtained for each model according to a second-degree polynomial equation, their statistical significance (based on a Student's t-test), the parameters measuring the correlation (R^2) and statistical significance (Fisher's F test) of the models. The value determined for R^2 for most of the variables was higher than 0.86, which would indicate that the model was adequate to represent the real relationships among the selected variables [22], but in some other cases this value was lower than 0.82. Moreover, the estimated significance levels confirm the regular fit of data. The values for each equation term were calculated in order to assess the contribution of their linear interaction, and quadratic effects of the independent variables. Employing the calculated significant regression coefficients at the 90% confidential level, two quadratic regression equations were set up, one for each output variable (y_1 -Swelling and y_2 -Lignin waste), for the six models. Hence, twelve equations were obtained in total Eq. 7-18:

(1) Vacuum XL + Air Drying (Vac-Air):

$$y_1(\text{Swelling \%}) = 778.78 + 40.67x_1 - 64.45x_2 - 344.30x_1^2 + 42.65x_2^2 - 16.27x_1x_2 \quad (7)$$

$$y_2(\text{Lignin Waste \%}) = 80.99 - 0.93x_1 - 3.34x_2 - 10.18x_1^2 - 2.91x_2^2 + 6.19x_1x_2 \quad (8)$$

(2) Vacuum XL + Vacuum Drying (Vac-Vac)

$$y_1(\text{Swelling \%}) = 1144.76 + 46.89x_1 - 146.12x_2 - 686.08x_1^2 + 100.40x_2^2 - 26.17x_1x_2 \quad (9)$$

$$y_2(\text{Lignin Waste \%}) = 80.99 - 0.93x_1 - 3.34x_2 - 10.18x_1^2 - 2.91x_2^2 + 6.19x_1x_2 \quad (10)$$

(3) 5 cycles of Freeze-Thawing XL + Air Drying (F-T x5-Air)

$$y_{1(\text{Swelling } \%)} = 902.17 - 56.45x_1 - 98.37x_2 - 241.29x_1^2 - 49.67x_2^2 + 4.41x_1x_2 \quad (11)$$

$$y_{2(\text{Lignin Waste } \%)} = 69.08 - 1.83x_1 - 10.58x_2 - 14.26x_1^2 + 0.03x_2^2 + 1.49x_1x_2 \quad (12)$$

(4) 5 cycles of Freeze-Thawing XL + Vacuum Drying (F-T x5-Vac)

$$y_{1(\text{Swelling } \%)} = 468.74 - 47.17x_1 + 60.89x_2 + 95.02x_1^2 - 105.90x_2^2 + 5.72x_1x_2 \quad (13)$$

$$y_{2(\text{Lignin Waste } \%)} = 69.08 - 1.83x_1 - 10.58x_2 - 14.26x_1^2 + 0.03x_2^2 + 1.49x_1x_2 \quad (14)$$

(5) 3 cycles of Freeze-Thawing XL + Air Drying (F-T x3-Air)

$$y_{1(\text{Swelling } \%)} = 552.83 - 37.92x_1 - 112.85x_2 + 55.44x_1^2 + 43.03x_2^2 + 219.24x_1x_2 \quad (15)$$

$$y_{2(\text{Lignin Waste } \%)} = 68.70 - 0.87x_1 - 7.15x_2 - 18.08x_1^2 + 1.91x_2^2 + 2.20x_1x_2 \quad (16)$$

(6) 3 cycles of Freeze-Thawing XL + Vacuum Drying (F-T x3-Vac)

$$y_{1(\text{Swelling } \%)} = 557.40 - 66.98x_1 - 0.96x_2 + 105.88x_1^2 - 52.12x_2^2 + 186.30x_1x_2 \quad (17)$$

$$y_{2(\text{Lignin Waste } \%)} = 68.70 - 0.87x_1 - 7.15x_2 - 18.08x_1^2 + 1.91x_2^2 + 2.20x_1x_2 \quad (18)$$

3.1.1. Influence of the input variables on the Swelling Capacity

For the Vac-Air synthesis pathway, the minimum value (376 %) was for experiment 3 while the maximum (909 %) was registered for experiment 4 (see Table 3). For the Vac-Vac synthesis route, the minimum was also for experiment 3 (455 %) whereas the maximum was for experiment 4 (1647 %) too. Based on these results, it could be observed that despite being the minimum and maximum values for the same experiments, the type of drying has an effect on the swelling capacity, in fact, vacuum drying enhances it. It is worth to mention that experiment 4 had a film-like shape, so the contact surface with water was higher and this is why it was so swollen. However, for the other two vacuum dried routes, vacuum reduced the subsequent swelling rate of the hydrogels. In the case of F-T x5-Air synthesis, the minimum was found on experiment 11

(513 %) and the maximum value was again for experiment 4 (970 %). At the F-T x5-Vac synthesis, the minimum was observed for experiment 4 (314 %) while the maximum value was for experiment 2 (656 %). The swelling ability for the F-T x3-Air experiments ranged from 367 to 968 %, being the minimum for the experiment 8 and the maximum for experiment 1. The values for F-T x3-Vac hydrogels were in the interval of 380-910 %, where the minimum value corresponded to experiment 4 whereas the maximum corresponded to experiment 1.

According to the regression coefficients (Table 5), it could be seen that the two input variables had an influence on the swelling capacity. Specifically, x_2 (PVA concentration) had a significant influence on this output variable, as well as the quadratic effect of x_1 (lignin concentration). The interaction between both input variables was also important in the case of the F-T x3-Air and F-T x3-Vac. The quadratic effect of x_2 presented a high influence on F-T x5-Vac synthesis. Ciolacu et al., (2017) and Yang et al., (2018) did also report that the swelling capacity depends on the composition of the hydrogels [18,23].

The surface plots for synthesis routes (1), (2) and (3) showed that for a fixed concentration of PVA, as lignin content was augmented, the swelling capacity of the hydrogel tended to increase (see Supplementary Data). However, after a certain concentration of lignin, the swelling capacity decreased. So, it was found that the maximum point was in between the extreme concentrations of lignin. It is also worth to mention that the swelling ability was displayed to be higher for lower PVA concentrations, but the response variable was much more influenced by the lignin content than by PVA one. This behavior could be due to the high influence of the quadratic term of lignin on the swelling equations [22]. The optimal conditions for routes (1), (2) and (3) were 15.8 % lignin and 5 % PVA, 15.5 % lignin and 5 % PVA and 13.7 % lignin and 5.3 % PVA, subsequently.

The surface plots for synthesis routes (4), (5) and (6) showed that for a fixed concentration of PVA, as lignin content was augmented, the swelling capacity of the hydrogel tended to decrease (see Supplementary Data). Nevertheless, after a certain concentration of lignin, the swelling capacity started to increase again. Therefore, the surfaces presented a minimum in between the

extreme contents of lignin and, therefore, the highest swelling capacities were found on the upper and lower concentration limits. Thus, the optimal conditions for the achievement of the highest swelling capacities following the routes (4), (5) and (6) were 5 % lignin and 8.8 % PVA, 5 % lignin and 5 % PVA and 5 % lignin and 5 % PVA, subsequently. In these three surfaces, however, no clear dominant variable was observed, since the quadratic terms did not have such a high significance level.

It was clearly seen that the addition of lignin did, in all cases, have a positive effect on the swelling properties of the PVA hydrogels. This fact was confirmed by the synthesis and characterization of the blank hydrogels, i.e., neat PVA hydrogels with concentrations of 5, 8 and 11 % PVA and the same crosslinking and drying pathways than the ones with lignin. In fact, the swelling ratio of these materials did not almost overpass the 350 %., This behaviour may be achieved to the size of the attached lignin molecules, since they are high molecular weight chains and they can lead to the creation of bigger pores, which can permit the penetration of more water molecules [18,24]. This fact would justify the incorporation of lignin into water absorbent polymeric materials. Ciolacu et al. also reported the same behaviour for their PVA-lignin chemically crosslinked hydrogels [18]. Yang et al. also confirmed that lignin improved the swelling ability of chitosan-PVA hydrogels [25].

3.1.2. Influence of the input variables on the Lignin Waste

The lignin waste of the 11 experiments in Vac-Air and Vac-Vac synthesis pathways were in the interval of 59-85 %. The minimum value was found for experiment 3 while the maximum was registered for experiment 5 (see Table 3). For the F-T x3-Air and F-T x3-Vac synthesis routes, the minimum was for experiment 11 (42 %) whereas the maximum was for experiment 7 (76 %). In the case of F-T x5-Air synthesis, the minimum was found on experiment 3 (44 %) and the maximum value was again on experiment 7 (76 %). It could be observed that the freeze-thawing method permits the retention of more lignin inside the matrix than the vacuum crosslinking. Moreover, the ranges in both freeze-thawing routes were very similar.

For the Vac-Air and Vac-Vac synthesis routes the most influencing regression coefficients on the lignin waste were the quadratic effect of x_1 and the interaction between both input variables x_1x_2 . In the other four synthesis pathways, the most significant regression coefficients were the quadratic effect of x_1 and x_2 (PVA concentration) itself. Therefore, it can be concluded that the PVA content directly affects lignin waste. To the best of our knowledge, no data has been collected within the literature about the lignin waste during the washing stage into account when characterizing hydrogels. Hence, this statement cannot be contrasted with any other work.

The surface plots for all synthesis routes showed that for a fixed concentration of PVA, as lignin content was augmented (see Supplementary Data), the lignin waste during the washing stage of the hydrogels tended to increase. This behaviour could be related to the addition of reactive sites and a higher crosslinking rate between both components. However, after a certain concentration of lignin, the lignin waste decreased. So, it could also be said here that the maximum points were found in between the extreme concentrations of lignin. It is also worth to mention that the swelling ability was tended to be higher for higher PVA concentrations; however, the response variable was much more influenced by the lignin content due to the significance level of its quadratic term. For the six routes, the optimal concentrations for the minimum lignin wastes were 5 % lignin and 11 % PVA (Vacuum XL, routes (1) and (2)), 25 % lignin and 11 % PVA (F-T x5 XL, routes (3) and (4)) and 5 % lignin and 11 % PVA (F-T x3 XL, routes (5) and (6)).

3.1.3. Optimization of the synthesis conditions and validation of the model

The objective of the optimization was to determine the formulations that would provide simultaneously the greatest swelling capacity and the lowest lignin waste during the washing stage via the six synthesis routes. Statgraphics Centurion XV software was used to carry out the optimization. For this aim, the values of the responses of each variable were converted using a desirability function. This function was considered to disclose the combination of the synthesis variables that maximize the swelling capacity and minimise the lignin waste at the same time.

The optimum conditions for the independent variables as well as the predicted and experimental results for the response variables are displayed in Table 4.

The suitability of the response surface methodology model for quantitative predictions could only be verified by the agreement of the predicted and experimental values in two of the six synthesis routes. The errors in the output swelling variable were higher than a 4 % in all the cases except for the two 5-times-freeze-thawed routes. However, the lowest errors in lignin waste were observed for the 3-times-freeze-thawed samples. The optimum formulations were repeated again in case the error was experimental, but similar results were obtained. Nevertheless, as the accuracy on swelling was considered more important than lignin waste and, as one of the aims of the optimization was to obtain the best synthesis route, the two via 5 freeze-thawing cycles were selected as the optimum pathways. Hence, the samples obtained via these two optimal routes were subjected to further characterization (namely 3 and 4 samples), together with their equivalent neat PVA hydrogels (namely 3.0 and 4.0). The swelling kinetics of these four samples is shown in Figure 3.

(Figure 3)

3.2. Hydrogel Characterization

3.2.1. Attenuated Total Reflection - Fourier Transformed Infrared Radiation (ATR-FTIR):

The two best optimal hydrogels (the ones obtained via the routes 3 and 4) were analyzed by FTIR technique. Figure 4 represents the spectra of both of them (namely 3 and 4) along with the spectra of neat PVA hydrogels (namely 3.0 and 4.0), commercial PVA and alkaline lignin. As it can be seen, there was no significant difference between both hydrogels without lignin, since the employed PVA was the same and the only difference was the quantity used for their synthesis. These hydrogels showed the characteristic peaks of commercial PVA (see Table 6), and the peak around 2855 cm^{-1} , which was a small shoulder in the commercial PVA spectrum, got intensified. This band corresponds to the stretching C–H from alkyl groups, as reported by Mansur et al. [26].

A peak did also appear at around 1545 cm^{-1} , which was attributed to C–O bondages, probably created when dissolving it into water [27].

As for the hydrogels containing lignin, there was not any notable variation between their spectra due to the use of identical components for their blends. The lignin hydrogels presented similar peaks to these shown by the neat PVA hydrogels, but some bands appeared or were shifted due to the interactions with alkaline lignin (see Table 7). The band around 2920 cm^{-1} , for example, lost intensity and was divided into two peaks at 2945 and 2916 cm^{-1} , probably due to the interactions with lignin, which presented two bands at 2947 and 2913 cm^{-1} . These bands correspond to alkyl asymmetric and aromatic C–H stretch vibrations, and also to the intramolecular hydrogen bonds. Moreover, the peak corresponding to the ester C=O bonds (at 1720 cm^{-1}) lost intensity, and the one belonging to the C=C stretch vibration at around 1570 cm^{-1} shifted to higher wavenumbers due to the intense band presented by lignin at 1597 cm^{-1} . The band appearing around 1545 cm^{-1} shifted to lower wavenumbers, probably due to the interactions with lignin, which presented a strong peak around 1513 cm^{-1} that corresponded to the C=C aromatic vibrations [28]. Around 1275 cm^{-1} , a shoulder did also appear, which could be related to the intense lignin peak at 1270 cm^{-1} and belonged to the guaiacyl units [29]. The band at 1100 cm^{-1} also got intensified, meaning that new C–C bonds might have been created and the peak at 840 cm^{-1} was enhanced too, which corresponded to C–O stretching vibrations.

The weak band at 618 cm^{-1} means that the commercial alkaline lignin contains carbon-sulphur bonds, which are characteristic of Kraft lignin [29].

(Figure 4)

3.2.2. Scanning Electron Microscopy (SEM):

SEM micrographs of the freeze-dried neat PVA and PVA-lignin hydrogels at two magnifications ($250\times$ and $2500\times$) are shown in Figure 5. For all the analyzed samples highly porous structures and different pore size distributions could be observed. However, it seemed that for the neat PVA hydrogels (Figures 5A-D) the morphology was more homogeneous than that for the lignin-PVA

hydrogel (Figures 5 E and F). In addition, some macro-pores did also appear on the sample without lignin that was vacuum-dried (sample 4.0, Figures 5 C and D), indicating that apart from the crosslinking method [16], the curing method also affected the morphology. This behaviour was also reported by Dominguez-Robles et al. [15] for straw alkaline lignin solved in soda and crosslinked with poly (methyl vinyl ether co-maleic acid). Thombare et al. [24] explained that the macro-pores often allow a facile penetration of water into the polymeric network, which would be the cause of a rapid initial swelling ability. Once the macro-pores have been filled, water starts to diffuse gradually through micro-pores. This could have happened in the case of the blank hydrogels, since they presented considerably big pores. However, this observation was not done here; in fact, lignin hydrogels presented a higher water swelling capacity in all cases (see Figure 3). Moreover, the walls that interconnect the micro voids amongst the sample with lignin are much smoother and brittle than the ones presented by neat PVA in samples 3.0 and 4.0. This microstructure in PVA can be associated to its strong intra and inter- molecular hydrogen bonds [30]. Yang et al. also described a similar result on the SEM characterization of their PVA/Chitosan hydrogels [25].

As deduced from the micrographs, the majority of the pores presented by neat PVA hydrogels were smaller than 1 μm , while the ones presented by lignin-based hydrogels were larger. This fact would confirm the previous statement about the size of the pores created due to the high molecular weight of lignin and its repercussion on the swelling capacity (Section 3.1.1.) [18]. Furthermore, unlike in the case of other authors [25], no lignin agglomerates were found in the SEM images, which confirmed the good miscibility between the components [31].

(Figure 5)

3.2.3. X-Ray Diffraction (XRD):

The X-Ray diffractograms for lignin, neat PVA hydrogels and lignin-PVA hydrogels are depicted in Figure 6. Neat PVA hydrogels presented their characteristic crystalline peaks. As previously reported [18,32], a strong peak was observed at $2\theta = 19.77^\circ$, which corresponded to the (101)

lattice plane, followed by a shoulder around 22.78° , corresponding to the (201) plane. Two weak peaks were also appreciated at 11.5° (attributed to the plane (100)) and 40.8° .

Lignin is an amorphous polymer and its diffractogram presented an intense broad peak at around 19° as shown in Figure 6. Goudarzy et al. also reported a similar maximum diffraction angle for softwood Kraft lignin [17]. As lignin was incorporated to the hydrogels, the semicrystalline structure of PVA was slightly modified although the main peaks did not disappear [18]. When lignin was added into the hydrogels, the strong signal at 19.77° was broadened, meaning that the crystalline regions of these hydrogels were lessened and the degree of crystallinity was, therefore, decreased. This fact was also confirmed by DSC analyses.

In order to calculate the mean size of the crystallites, which are the ordered domains in a polymer, Scherrer's equation was employed (Eq. 4). Measuring the width at half of the main crystalline peak, the estimated crystallite size for both blank and lignin-hydrogels was lower than 5 nm. In addition, the notably wide peak of the lignin would mean that the crystallite size was significantly smaller than the ones in the hydrogels, since lignin is an amorphous biopolymer and usually has few ordered domains. Thus, the only conclusion we could get from these results was that all the crystallites were smaller than 5 nm and that the values calculated by any crystallinity equation would not be representative for the samples [33], although some authors have published these results [17,18].

(Figure 6)

3.2.4. Differential Scanning Calorimetry (DSC):

DSC analyses were performed in order to analyze the thermal properties of the synthesized hydrogels. The results for the analyzed parameters during the cooling and the second heating stages (T_c , ΔH_c , T_g , T_m , ΔH_m and χ_c) are summarized in Table 8, and the DSC curves for these stages are also shown in Figure 7.

After removing the thermal history of the samples with the first heating scan, the appearance of a single T_g indicated a good blend miscibility [25], as previously observed in the SEM micrographs. This fact was noticed in all the analysed hydrogels. For neat PVA hydrogels (samples 3.0 and 4.0), the T_g values were similar (73.10 and 68.24 °C, successively). When lignin was incorporated into the samples, for hydrogels 3 and 4, the T_g values increased up to around 85 °C. This could be a consequence of the interactions such as hydrogen bonds between PVA and lignin, which could have restricted the chain mobility [19].

The T_m also got modified with the addition of lignin. Neat PVA hydrogels melted at around 236 °C, while the hydrogels containing lignin presented the fusion peak at around 230 °C. This behaviour is also an evidence of the good miscibility of the components [19]. As for the crystallization temperature (T_c), the addition of lignin also caused a decrease on it. In fact, the T_c of the neat PVA samples was placed around 205 °C and the one for the hydrogels with lignin at around 195 °C. Moreover, the crystallization enthalpy was also diminished from around 55 and 58 J/g (for samples 3.0 and 4.0, subsequently) to 27 and 41 J/g for samples 3 and 4, subsequently. This was attributed to the diminution of the crystalline regions as lignin was incorporated, which was also confirmed by the reduction on the melting enthalpy at the second heating scan. Thus, the degree of crystallinity (χ_c) was calculated from the latest data and Eq. 5,. The results confirm that χ_c decreased with lignin addition [19], since the values for neat PVA samples (21.63 and 23.04 % for samples 3.0 and 4.0, subsequently) were around 1.5 % higher than the ones for the lignin samples (20.10 and 21.56 % for samples 3 and 4, subsequently). Moreover, the crystallinity degrees of the samples 3 and 3.0 were below the ones reported for 4 and 4.0, probably due to a lower PVA content and higher lignin content in the case of sample 3. However, it is important to bear in mind that these values derive from the second heating scan, so the initial crystallinity would be slightly higher. These results were in accordance with the ones obtained from XRD analysis. As previously reported [31], it is known that when an amorphous polymer is blended with a semicrystalline polymer, the degree of its crystallinity decreases, and this statement was also confirmed in this case.

(Figure 7)

3.2.5. Thermogravimetric Analysis (TGA):

TG and DTG curves of lignin, neat PVA hydrogels and lignin-PVA hydrogels are shown in Figure 8A and 8B. The onset and maximum degradation temperatures, as well as the char residue at the end of the test are summarized in Table 9. Thermogravimetric studies were done in order to investigate the effect of lignin on the degradation of the blended hydrogels. For neat PVA hydrogels (3.0 and 4.0), four weight loss stages were observed. The first one appeared at around 150 °C and it was attributed to the evaporation of the adsorbed bound water [25]. A second stage was detected at around 250 °C, which still left an 85 % of residue and belonged to the initial degradation of the polymer. The maximum weight loss and, hence, the major degradation was viewed at around 375 °C, corresponding to the depolymerization of the acetylated and deacetylated units of the polymer [25]. This stage was followed by another weight loss at 440 °C, achieved to the thermal degradation of some by-products generated by PVA, and a final residue of around 2.6 % was accounted [25].

Commercial alkaline lignin presented a constant weight loss; however, the temperature of the maximum degradation was registered at 380 °C. No other significant degradation stages were detected and the final residue left was high, since it was almost of 40 %. This implies that commercial alkaline lignin has many inorganic impurities, and would confirm the possibility of containing carbon-sulphur traces, as previously stated in Section 3.2.1.

When lignin was incorporated, the hydrogels presented three main weight loss stages, but there was a fourth stage which overlapped with the second one, as shown in Figure 8B. The first stage was observed at around 120 °C and it was as well attributed to moisture evaporation. The main degradation stage appeared around 330 °C, but it was overlapped with the one at 280 °C. This loss might have been the one appearing at 250 °C in the case of neat PVA, but as lignin was incorporated, the thermal stability was enhanced and, hence, it could have shifted to higher temperatures. Hu et al. [34] explained this behaviour as the possible introduction of aromatic

structures of lignin into PVA chains via strong hydrogen bonds. After the main degradation step, another loss was detected around 430 °C, which was shifted to a lower temperature than in the previous case. The residue left for both lignin hydrogels was between 14-20 %, which was directly related to lignin.

(Figure 8)

3.2.6. Compression Tests:

The compression tests of the samples were studied and the calculated data from the stress-strain curves for compression to 80 % of the initial thickness are shown in Table 10. At the maximum deformation, none of the samples was broken; in fact, all the samples had an excellent ability of integrity and recovery. This could be due to the accommodation of the stress by the rearrangement of the polymeric chains and the retractable elastic forces developed consequently [6]. Nevertheless, there were some variations in the estimated modulus. For the blank hydrogels (3.0 and 4.0) the reported moduli were of around 77.6 and 41.7 MPa, respectively. When lignin was added to the samples, the modulus decreased to around 18.8 and 29.2 MPa for samples 3 and 4, subsequently. Therefore, as lignin was incorporated, the moduli of the hydrogels were reduced despite the different drying method, making the samples less rigid. This could be related with the pore-size of the samples and would confirm what was concluded for the swelling capacity; in other words, when lignin was blended with PVA, greater pores were generated due to the reduction of interactions within PVA which, at the same time, enhanced the adsorption of water and made the hydrogel less compact and rigid [25]. Nonetheless, the obtained modulus for the PVA-lignin samples would be high enough to support the weight of soil layers if the final application was agricultural, for instance.

4. Conclusions

The optimization of the synthesis conditions of lignin-based PVA hydrogels was successfully carried out employing a three-level-two-factorial design. The statistical analysis showed that the PVA and lignin concentrations had great impact on the lignin waste during the washing stage and

on the swelling capacity of the synthesized hydrogels. The selected optimum synthesis routes enabled the obtaining of physically crosslinked hydrogels with up to 800 % water retention ability and a lignin waste between 40-50 %. The interactions between lignin and PVA were confirmed by the shifts and modifications on the FTIR bands. The SEM images permitted the observance of a different porous microstructure when lignin was added, which was responsible of the high swelling capacity. XRD analyses indicated the disappearance of some crystalline regions as amorphous lignin was incorporated, which was also confirmed by DSC and TGA techniques. Compression tests showed that, although Young's modulus was more than halved as lignin content increased, all the hydrogels kept complete integrity even compressing them up to an 80 % of their initial thickness. In conclusion, physically crosslinked greener lignin hydrogels were synthesized via two methods, which had great water retention capacities as well as good thermal and mechanical properties, meaning they could be applied in many fields.

Acknowledgements

The authors would like to acknowledge the financial support of the Department of Education of the Basque Government (IT1008-16). A. Morales would like to thank the University of the Basque Country (Training of Researcher Staff, PIF17/207). P. Gullón would like to express her gratitude to MINECO for financial support (Grant reference IJCI-2015-25304). The authors thank for technical and human support provided by SGIker (UPV/EHU/ ERDF, EU).

References

- [1] S. Laurichesse,, L. Avérous, *Prog. Polym. Sci.* 39(7) (2014) 1266–90.
10.1016/j.progpolymsci.2013.11.004.
- [2] V.K. Thakur,, M.K. Thakur, *Int. J. Biol. Macromol.* 72 (2015) 834–47.
10.1016/j.ijbiomac.2014.09.044.
- [3] M.H. Sipponen,, H. Lange,, C. Crestini,, A. Henn,, M. Österberg, *ChemSusChem* 12(10) (2019) 2038. 10.1002/cssc.201901218.

- [4] V.K. Thakur,, M.K. Thakur,, P. Raghavan,, M.R. Kessler, *ACS Sustain. Chem. Eng.* 2(5) (2014) 1072–92. 10.1021/sc500087z.
- [5] M. Mahinroosta,, Z. Jomeh Farsangi,, A. Allahverdi,, Z. Shakoori, *Mater. Today Chem.* 8 (2018) 42–55. 10.1016/j.mtchem.2018.02.004.
- [6] M.R. Guilherme,, F.A. Aouada,, A.R. Fajardo,, A.F. Martins,, A.T. Paulino,, M.F.T. Davi,, A.F. Rubira,, E.C. Muniz, *Eur. Polym. J.* 72 (2015) 365–85. 10.1016/j.eurpolymj.2015.04.017.
- [7] L. Voorhaar,, R. Hoogenboom, *Chem. Soc. Rev.* 45(14) (2016) 4013–31. 10.1039/c6cs00130k.
- [8] P. Vashisth,, V. Pruthi, *Mater. Sci. Eng. C* 67 (2016) 304–12. 10.1016/j.msec.2016.05.049.
- [9] M. Li,, X. Jiang,, D. Wang,, Z. Xu,, M. Yang, *Colloids Surfaces B Biointerfaces* 177(September 2018) (2019) 370–6. 10.1016/j.colsurfb.2019.02.029.
- [10] Y. Geng,, X.Y. Lin,, P. Pan,, G. Shan,, Y. Bao,, Y. Song,, Z.L. Wu,, Q. Zheng, *Polymer (Guildf)*. 100 (2016) 60–8. 10.1016/j.polymer.2016.08.022.
- [11] B. Gyarmati,, B.Á. Szilágyi,, A. Szilágyi, *Eur. Polym. J.* 93(March) (2017) 642–69. 10.1016/j.eurpolymj.2017.05.020.
- [12] Z. Gao,, L. Duan,, Y. Yang,, W. Hu,, G. Gao, *Appl. Surf. Sci.* 427 (2018) 74–82. 10.1016/j.apsusc.2017.08.157.
- [13] A. Oryan,, A. Kamali,, A. Moshiri,, H. Baharvand,, H. Daemi, *Int. J. Biol. Macromol.* (2017). 10.1016/j.ijbiomac.2017.08.184.
- [14] S. Park,, S.H. Kim,, J.H. Kim,, H. Yu,, H.J. Kim,, Y.H. Yang,, H. Kim,, Y.H. Kim,, S.H. Ha,, S.H. Lee, *J. Mol. Catal. B Enzym.* 119 (2015) 33–9. 10.1016/j.molcatb.2015.05.014.

- [15] J. Domínguez-Robles,, M.S. Peresin,, T. Tamminen,, A. Rodríguez,, E. Larrañeta,, A.S. Jääskeläinen, *Int. J. Biol. Macromol.* 115 (2018) 1249–59.
10.1016/j.ijbiomac.2018.04.044.
- [16] A. Kumar,, S.S. Han, *Int. J. Polym. Mater. Polym. Biomater.* 66(4) (2017) 159–82.
10.1080/00914037.2016.1190930.
- [17] A. Goudarzi,, L.-T. Lin,, F.K. Ko, *J. Nanotechnol. Eng. Med.* 5(2) (2014) 021006.
10.1115/1.4028300.
- [18] D. Ciolacu,, G. Cazacu, *J. Nanosci. Nanotechnol.* 18(4) (2018) 2811–22.
10.1166/jnn.2018.14290.
- [19] X. He,, F. Luzi,, X. Hao,, W. Yang,, L. Torre,, Z. Xiao,, Y. Xie,, D. Puglia, *Int. J. Biol. Macromol.* 127 (2019) 665–76. 10.1016/j.ijbiomac.2019.01.202.
- [20] S.A. Bencherif,, A. Srinivasan,, F. Horkay,, J.O. Hollinger,, K. Matyjaszewski,, N.R. Washburn, *Biomaterials* 29(12) (2008) 1739–49. 10.1016/j.biomaterials.2007.11.047.
- [21] M.N. Collins,, C. Birkinshaw, *J. Mater. Sci. Mater. Med.* 19(11) (2008) 3335–43.
10.1007/s10856-008-3476-4.
- [22] B. Gullón,, P. Gullón,, T.A. Lú-Chau,, M.T. Moreira,, J.M. Lema,, G. Eibes, *Ind. Crops Prod.* 108(April) (2017) 649–59. 10.1016/j.indcrop.2017.07.014.
- [23] M. Yang,, M.S.U. Rehman,, T. Yan,, A.U. Khan,, P. Oleskowicz-Popiel,, X. Xu,, P. Cui,, J. Xu, *Bioresour. Technol.* 249(October 2017) (2018) 737–43.
10.1016/j.biortech.2017.10.055.
- [24] N. Thombare,, S. Mishra,, M.Z. Siddiqui,, U. Jha,, D. Singh,, G.R. Mahajan, *Carbohydr. Polym.* 185(October 2017) (2018) 169–78. 10.1016/j.carbpol.2018.01.018.
- [25] W. Yang,, E. Fortunati,, F. Bertoglio,, J.S. Owczarek,, G. Bruni,, M. Kozanecki,, J.M. Kenny,, L. Torre,, L. Visai,, D. Puglia, *Carbohydr. Polym.* 181(October 2017) (2018)

- 275–84. 10.1016/j.carbpol.2017.10.084.
- [26] H.S. Mansur,, C.M. Sadahira,, A.N. Souza,, A.A.P. Mansur, Mater. Sci. Eng. C 28(4) (2008) 539–48. 10.1016/j.msec.2007.10.088.
- [27] S. Karimi,, J. Feizy,, F. Mehrjo,, M. Farrokhnia, RSC Adv. 6(27) (2016) 23085–93. 10.1039/c5ra25983e.
- [28] A. Morales,, B. Gullón,, I. Dávila,, G. Eibes,, J. Labidi,, P. Gullón, Ind. Crops Prod. 124 (2018). 10.1016/j.indcrop.2018.08.032.
- [29] S. Sathawong,, W. Sridach,, K.A. Techato, J. Environ. Chem. Eng. 6(5) (2018) 5879–88. 10.1016/j.jece.2018.05.008.
- [30] L.Y. Wang,, M.J. Wang, ACS Sustain. Chem. Eng. 4(5) (2016) 2830–7. 10.1021/acssuschemeng.6b00336.
- [31] K.J. Lee,, J. Lee,, J.Y. Hong,, J. Jang, Macromol. Res. 17(7) (2009) 476–82. 10.1007/BF03218895.
- [32] H. Dai,, H. Zhang,, L. Ma,, H. Zhou,, Y. Yu,, T. Guo,, Y. Zhang,, H. Huang, Carbohydr. Polym. 209(381) (2019) 51–61. 10.1016/j.carbpol.2019.01.014.
- [33] A. Morales,, M.Á. Andrés,, J. Labidi,, P. Gullón, Ind. Crops Prod. 131 (2019). 10.1016/j.indcrop.2019.01.071.
- [34] X.-Q. Hu,, D.-Z. Ye,, J.-B. Tang,, L.-J. Zhang,, X. Zhang, RSC Adv. 6(17) (2016) 13797–802. 10.1039/C5RA26385A.
- [35] E. Larrañeta,, M. Imízcoz,, J.X. Toh,, N.J. Irwin,, A. Ripolin,, A. Perminova,, J. Domínguez-Robles,, A. Rodríguez,, R.F. Donnelly, ACS Sustain. Chem. Eng. 6(7) (2018) 9037–46. 10.1021/acssuschemeng.8b01371.
- [36] L. Musilová,, A. Mráček,, A. Kovalcik,, P. Smolka,, A. Minařík,, P. Humpolíček,, R.

Vícha,, P. Ponížil, Carbohydr. Polym. 181(October 2017) (2018) 394–403.

10.1016/j.carbpol.2017.10.048.

[37] H. Bian,, L. Jiao,, R. Wang,, X. Wang,, W. Zhu,, H. Dai, Eur. Polym. J. 107(August) (2018) 267–74. 10.1016/j.eurpolymj.2018.08.028.

[38] K. Ravishankar,, M. Venkatesan,, R.P. Desingh,, A. Mahalingam,, B. Sadhasivam,, R. Subramaniam,, R. Dhamodharan, Mater. Sci. Eng. C 102(January) (2019) 447–57. 10.1016/j.msec.2019.04.038.

Tables

Table 1: Literature overview about hydrogels with lignin and their applications.

Crosslinking type	Interactions	Type of hydrogel	Polymers	Applications	References
Chemical	Ester bondages	Synthetic polymer based	Poly (methyl vinyl ether co-maleic acid) and different technical lignins	Water purification	[15]
Chemical	Ester bondages	Synthetic polymer based	Lignin and poly(ethylene glycol)/ poly(methyl vinyl ether-co-maleic acid)	Drug delivery	[35]
Chemical	Chemical Crosslinker	Polysaccharide-based	Glycinated Kraft lignin and Hyaluronan	Tissue engineering	[36]
Chemical	Chemical Crosslinker	Synthetic polymer based	Poly (vinyl alcohol), Cellulose nanofibrils and lignin	Pressure sensors	[37]
Chemical	Chemical Crosslinker	Polysaccharide-based	Agarose and Kraft lignin	Non determined	[29]
Physical	Co-dissolution in 1-ethyl-3-methylimidazolium acetate	Polysaccharide- based beads	Cellulose and lignin	Lipase immobilizers	[14]
Physical	Electrostatic interactions	Polysaccharide-based	Chitosan and lignin	Scaffolds in tissue engineering	[38]

Table 2: Experimental design.

Experiment #	x₁	x₂	Alkaline Lignin (% w/w)	PVA (% w/w)
1	-1	-1	5	5
2	-1	0	5	8
3	-1	1	5	11
4	0	-1	15	5
5	0	0	15	8
6	0	0	15	8
7	0	0	15	8
8	0	1	15	11
9	1	-1	25	5
10	1	0	25	8
11	1	1	25	11

Table 3: Values of the response variables for the six synthesis paths.

	(1) Vac-Air		(2) Vac-Vac		(3) F-T x5-Air		(4) F-T x5-Vac		(5) F-T x3-Air		(6) F-T x3-Vac	
	Swelling (%)	Ligning Waste (%)	Swelling (%)	Ligning Waste (%)	Swelling (%)	Ligning Waste (%)	Swelling (%)	Ligning Waste (%)	Swelling (%)	Ligning Waste (%)	Swelling (%)	Ligning Waste (%)
E1	454.52	77.90	467.93	77.90	732.94	77.90	411.06	77.90	968.07	68.90	910.01	68.90
E2	435.68	72.43	512.54	72.43	757.72	72.43	656.48	72.43	659.40	44.89	712.96	44.89
E3	376.51	59.03	455.68	59.03	562.00	59.03	553.42	59.03	397.16	44.49	463.58	44.49
E4	909.86	79.82	1647.59	79.82	970.53	79.82	314.48	79.82	779.88	68.08	380.05	68.08
E5	754.12	85.15	1172.55	85.15	905.98	85.15	434.21	85.15	584.94	66.49	674.16	66.49
E6	764.04	80.53	947.88	80.53	965.14	80.53	473.91	80.53	532.82	71.26	627.44	71.26
E7	806.91	80.81	1256.51	80.81	865.27	80.81	537.01	80.81	584.92	76.28	479.17	76.28
E8	744.23	72.79	900.06	72.79	704.59	72.79	372.25	72.79	367.62	65.20	521.91	65.20
E9	604.65	66.15	686.14	66.15	666.55	66.15	370.30	66.15	489.03	60.14	440.44	60.14
E10	444.50	65.63	462.15	65.63	534.15	65.63	432.10	65.63	512.94	48.40	505.00	48.40
E11	461.56	72.02	569.20	72.02	513.25	72.02	535.53	72.02	795.10	44.52	739.20	44.52

Table 4: Optimal conditions and predicted/experimental values for the response variables.

Synthesis Route	Alkaline Lignin (% w/w)	PVA (% w/w)	Predicted Value		Experimental Average Value		Error (%)	
			Swelling (%)	Ligning Waste (%)	Swelling (%)	Ligning Waste (%)	Swelling (%)	Ligning Waste (%)
(1)	23.02	5	710.29	69.17	345.30	81.16	51.39	-17.34
(2)	22.26	5	1083.59	70.88	199.26	82.75	81.61	-16.74
(3)	9.12	9.87	770.14	58.11	789.89	51.94	-2.57	10.63
(4)	5	10.39	587.82	49.09	567.06	41.06	3.53	16.35
(5)	25	11	719.77	46.71	659.67	45.77	8.35	2.02
(6)	25	11	729.51	46.71	547.93	44.12	24.90	5.55

Table 5: Regression coefficients and statistical parameters measuring the correlation and significance of the models.

	(1) Vac-Air		(2) Vac-Vac		(3) F-T x5-Air		(4) F-T x5-Vac		(5) F-T x3-Air		(6) F-T x3-Vac	
	y1	y2	y1	y2								
β_0	778.78	80.99	1144.76	80.99	902.17	69.08	468.74	69.08	552.83	68.70	557.40	68.70
β_1	40.67 ^b	-0.93	46.89	-0.93	-56.45	-1.83	-47.17	-1.83	-37.92	-0.87	-66.98	-0.87
β_2	-64.45 ^a	-3.34	-146.12	-3.34	-98.37 ^b	-10.58 ^a	60.89 ^c	-10.58 ^a	-112.85 ^b	-7.15 ^c	-0.96	-7.15 ^c
β_{11}	-344.30 ^a	-10.18 ^a	-686.08 ^a	-10.18 ^a	-241.29 ^a	-14.26 ^a	95.02 ^c	-14.26 ^a	55.44	-18.08 ^b	105.88	-18.08 ^b
β_{22}	42.65	-2.91	100.40	-2.91	-49.67	0.03	-105.90 ^c	0.03	43.03	1.91	-52.12	1.91
β_{12}	-16.27	6.19 ^b	-26.17	6.19 ^b	4.41	1.49	5.72	1.49	219.24 ^a	2.20	186.30 ^b	2.20
R^2	0.98	0.92	0.86	0.92	0.93	0.90	0.76	0.90	0.89	0.82	0.77	0.82
F-exp	50.93	11.12	5.96	11.12	13.53	9.22	3.24	9.22	8.467	4.44	3.32	4.44
S.L.* (%)	99.97	99.03	96.39	99.03	99.37	98.54	88.87	98.54	98.24	93.61	89.29	93.61

^a Significant coefficients at the 99 % confidence level.

^b Significant coefficients at the 95 % confidence level.

^c Significant coefficients at the 90 % confidence level.

* Significance Level

Table 6: Characteristic FTIR peaks of PVA.

Wavenumber (cm⁻¹)	Assignment
3300	-OH stretch vibration
2920	Alkyl asymmetric C-H stretch vibration
2855	Symmetric C-H stretch vibration
1720	Ester C=O stretch vibration
1660	Residual C=O stretch vibration
1560	C=C stretch vibration
1425	CH ₂ bending vibration
1325	O-H deformation vibration
1100	C-C stretching vibration
840	C-C and C-O stretching vibration

Table 7: Characteristic FTIR peaks of alkaline lignin.

Wavenumber (cm⁻¹)	Assignment
3215	-OH stretch vibration
2947	Alkyl asymmetric vibration
2913	Aromatic C-H stretching vibration
1679	C=O ester bonds
1597	C=C stretch vibration
1513	C=C aromatic vibrations
1456	C-H bonds of the methyl groups
1429	C-H bonds of the methyl groups
1269	Guaiacyl units
1100	C-C bonds
1030	C-O stretching vibration
865	C-C stretching vibration
821	aromatic -CH out of plane vibration
618	C-S bonds

Table 8: Summarized results for the analyzed parameters by DSC and calculations.

Sample	Cooling Scan			2 nd Heating Scan					
	T _c (°C)	ΔH _c (W·°C/g)	ΔH _c (J/g)	T _g (°C)	T _m (°C)	ΔH _m (W·°C/g)	ΔH _m (J/g)	m _{filler} (%)	χ _c (%)
3.0	204.50	18.29	54.87	76.43	236.53	11.65	34.95	0	21.63
4.0	205.93	19.30	57.90	79.37	235.90	12.41	37.23	0	23.04
3	195.30	8.90	26.70	87.07	228.63	7.81	23.43	0.28	20.10
4	198.17	13.80	41.40	88.80	230.43	9.22	27.66	0.21	21.56

T_c: Crystallization temperature; T_g: Glass transition temperature; ΔH_m: Melting enthalpy; χ_c: Crystallinity degree; ΔH_c: Crystallization enthalpy; T_m: Melting temperature; m_{filler}: filler mass percentage

Table 9: Onset and maximum degradation temperatures and residue after TGA.

Sample ID	T_{onset} (°C)	T_{max} (°C)	Residue (%)
AL	172.0	380.0	39.0
3.0	225.0	372.5	2.7
4.0	230.5	374.0	2.6
3	217.0	323.0	19.5
4	223.0	334.5	14.7

Table 10: Results for the compression tests of the samples.

Sample	Young's Compression Modulus (MPa)	Standard Deviation (MPa)
3.0	77.57	8.40
4.0	41.64	3.42
3	18.75	0.53
4	29.21	6.18

Figure list

Figure 1: Diagram of the experimental procedure of the hydrogel synthesis.

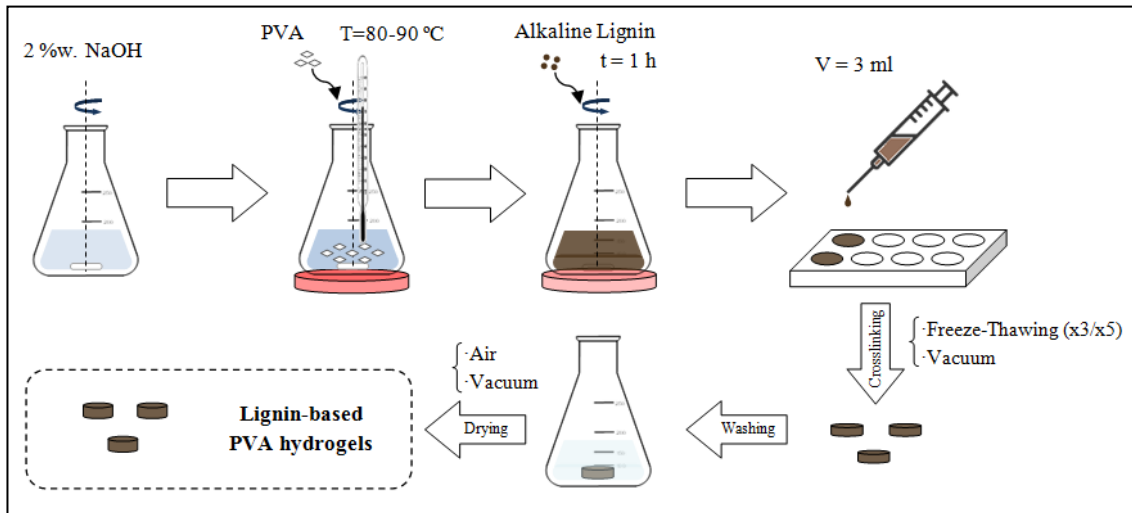


Figure 2: Scheme of the six hydrogel synthesis pathways.

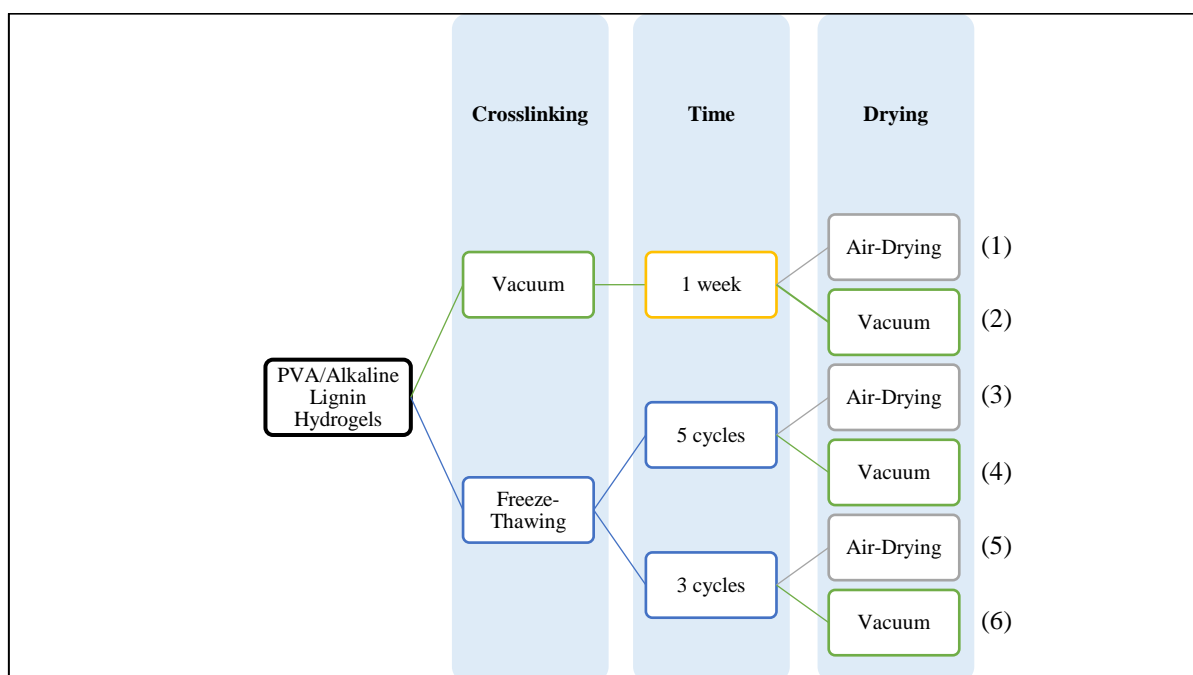


Figure 3: Swelling performance of the hydrogels during the first 48 h.

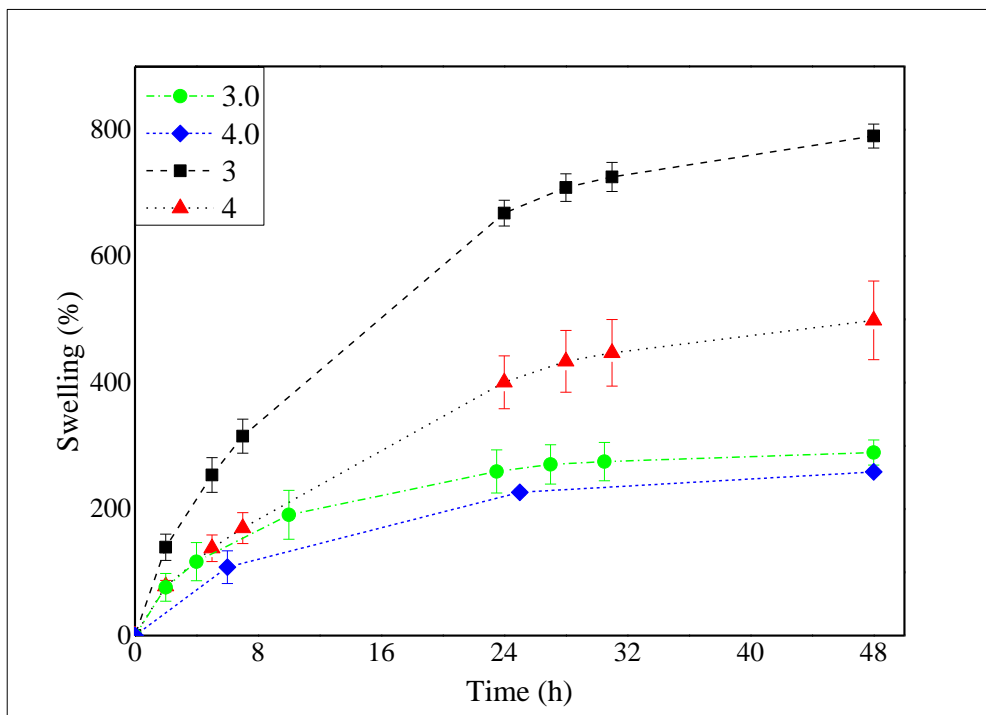


Figure 4: FTIR of commercial PVA, commercial alkaline lignin and the selected hydrogels with (samples 3 and 4) and without lignin (samples 3.0 and 4.0).

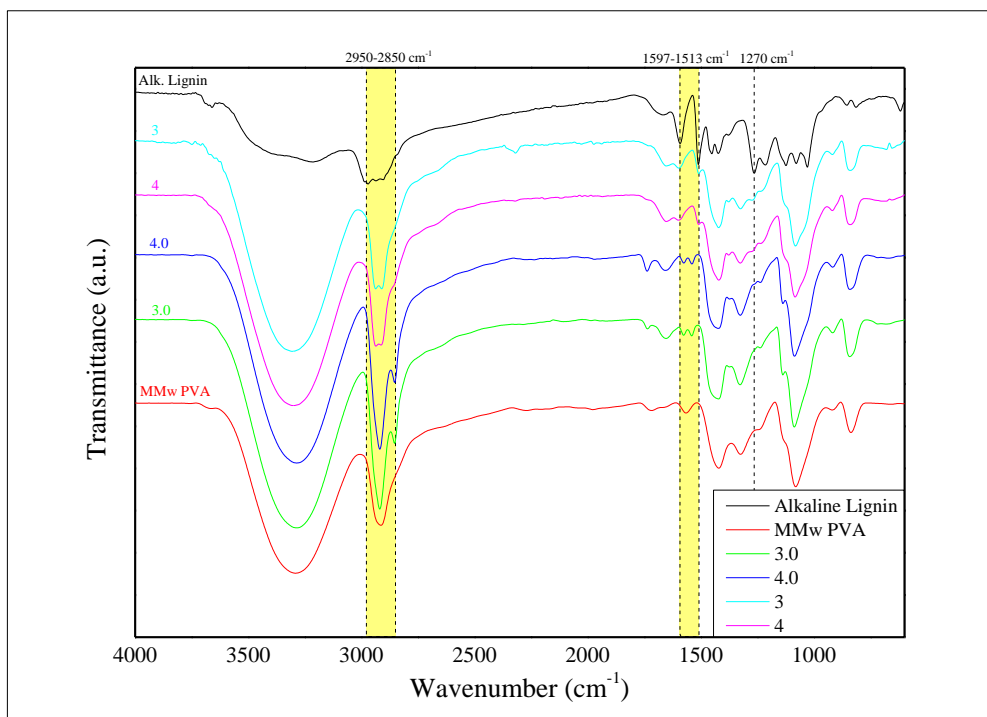


Figure 5: SEM micrographs of the samples 3.0, 4.0 and 4 at 250x (A, C and E) and 2500x (B, D and F) magnifications.

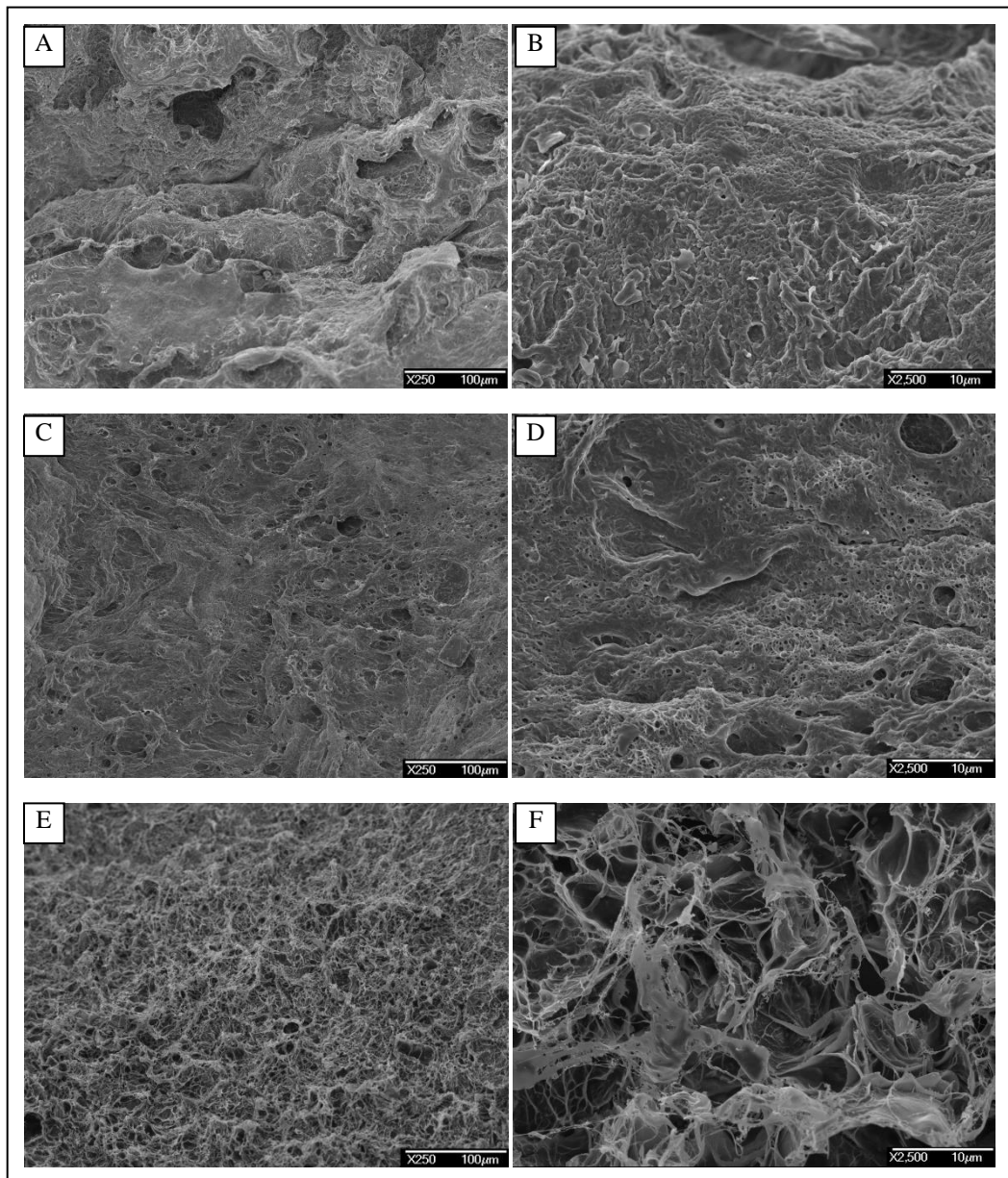


Figure 6: XRD diffractograms of the hydrogels 3.0, 4.0, 3, 4 and commercial alkaline lignin.

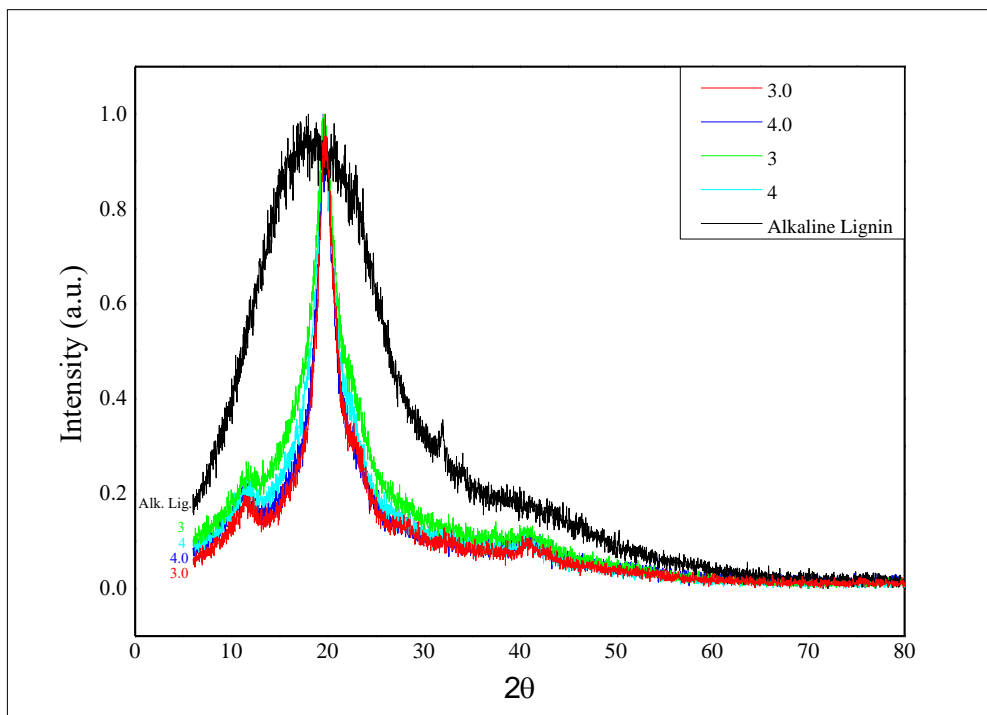


Figure 7: DSC thermograms of the first cooling stage and second heating stage of hydrogels 3.0, 4.0, 3, 4 and commercial alkaline lignin.

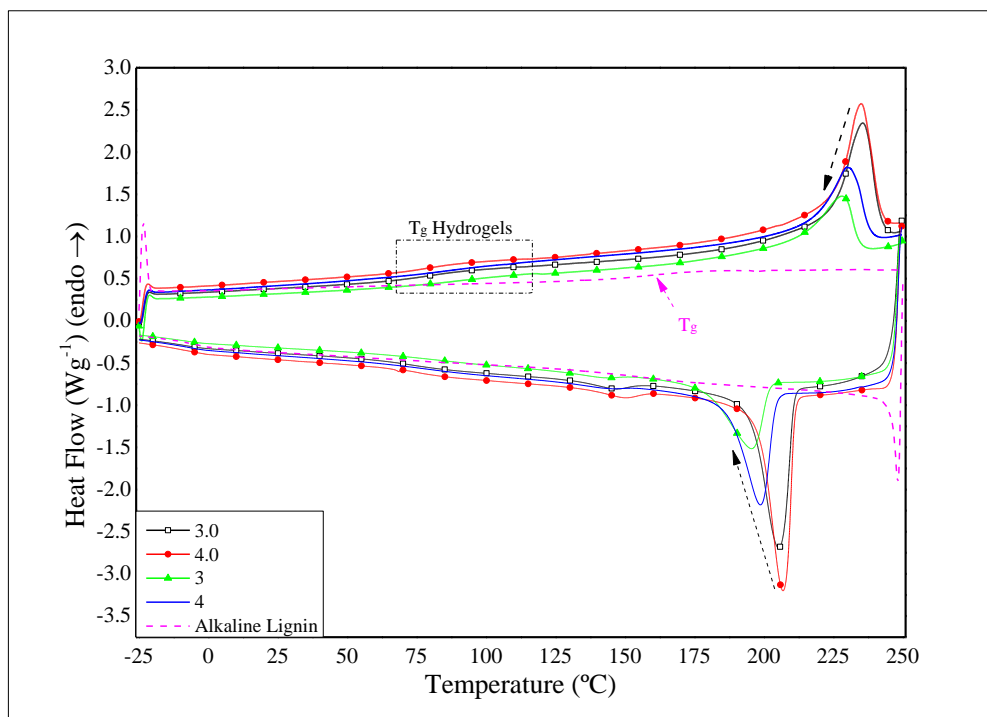


Figure 8: (A) TG and (B) DTG curves of hydrogels 3.0, 4.0, 3, 4 and commercial alkaline lignin.

